Recoil isomer tagging in the proton-rich odd-odd $N=77$ isotones, $^{142}_{65}$Tb and $^{144}_{67}$Ho

C. Scholey, D. M. Cullen,* E. S. Paul, A. J. Boston, P. A. Butler, T. Enqvist, C. Fox, H. C. Scraggs, S. L. Shepherd, and O. Stezowski†
Oliver Lodge Laboratory, Department of Physics, University of Liverpool, Liverpool L69 7ZE, United Kingdom

A. M. Bruce
School of Engineering, University of Brighton, Brighton BN2 4GJ, United Kingdom

P. M. Walker, M. Caamaño, and J. Garcés Narro
Department of Physics, University of Surrey, Guildford, Surrey GU2 7XH, United Kingdom

M. A. Bentley and D. T. Joss
School of Sciences, Staffordshire University, Stoke-on-Trent ST4 2DE, United Kingdom

O. Dorvaux,‡ P. T. Greenlees, K. Helariutta,§ P. M. Jones, R. Julin, S. Juutinen, H. Kankaanpää, H. Kettunen, P. Kuusiniemi, M. Leino, M. Muikku, P. Nieminen, P. Rahkila, and J. Uusitalo
Department of Physics, University of Jyväskylä, P.O. Box 35, FIN-40351 Jyväskylä, Finland
(Received 13 September 2000; published 21 February 2001)

A fusion-evaporation reaction has been employed to search for isomeric states in the near-proton drip-line $N=77$ isotones, $^{142}_{65}$Tb and $^{144}_{67}$Ho. The recoiling nuclei were implanted into a silicon detector at the focal plane of a gas-filled separator, where a recoil isomer tagging technique was employed to correlate prompt and delayed γ-ray transitions across isomeric states. New states were observed to be built upon a known 15-μs isomer in ^{142}Tb and the feeding and decay of a new 500(20)-ns isomeric state was established in ^{144}Ho. This measurement represents the first observation of excited states in ^{144}Ho. The behavior of the new states above the isomers suggests that they are built upon low-deformation configurations with significant triaxiality. This is in contrast to the lighter-mass proton emitters that were recently interpreted as being well-deformed, prolate, axially symmetric nuclei.

DOI: 10.1103/PhysRevC.63.034321 PACS number(s): 21.10.Re, 23.20.Lv, 27.60.+j

I. INTRODUCTION

The mass 130–140 region of nuclei, near the proton drip line, is currently the subject of a considerable amount of theoretical attention. This activity has been directed toward the understanding of proton radioactivity [1] that was recently observed in ^{140}Ho, ^{141}Ho, and ^{131}Eu [2,3]. In these nuclei, the proton decay rates are explained in terms of a single proton tunneling through a Coulomb plus centrifugal barrier using the WKB approximation and spectroscopic factors derived from low-seniority *deformed* shell-model calculations [2–5]. In contrast, the proton decay rates in the heavier nuclei from Z=69 (Tm) to Z=81 (Tl) have been described by calculations based on *spherical* shell-model calculations [6]. In order to add experimental validation to the predictions that these proton drip-line nuclei can be deformed, it would be useful to observe excited states in the parent nuclei. The mass 130–140 drip-line nuclei have, however, proven to be very difficult to access and study at moderate spins using heavy-ion fusion-evaporation reactions with stable beam and target combinations. In this region, evaporation residues that are less neutron deficient are unavoidably produced with larger cross sections than the other nuclei of interest. The reason that ^{140}Ho, ^{141}Ho, and ^{131}Eu could be studied [1,33] relies on the fact that these channels can be selectively tagged by the observation of a proton decay with a specific energy. For the other nuclei in this region that do not proton decay, this method cannot be exploited and therefore, a systematic study of the evolution of nuclear deformation with mass, cannot be undertaken using proton tagging alone.

In order to complement the information obtained from proton-decay measurements and extend the experimental knowledge of this proton-rich region, another tagging method is required to preferentially select the nuclei of interest. The tagging method employed in this work requires the presence of an isomeric state that decays by γ-ray emission. Isomeric states are not uncommon in this region and indeed proton emission was recently observed from an isomeric state in ^{141m}Ho [3]. Such isomers are a result of the high-j states that involve the $h_{11/2}$ intruding proton orbit and their associated high-multipolarity decays. In addition, the $h_{11/2}$ proton orbits tend to favor collective prolate deformed

*Present address: Department of Physics and Astronomy, University of Manchester, Manchester M13 9PL, United Kingdom.
†Present address: Institut de Physique Nucléaire de Lyon, IN2P3/CNRS, Université C. Bernard Lyon-1, F-69622 Villeurbanne Cedex, France.
‡Present address: Institut de Recherches Subatomique, CNRS-IN2P3, 23 Rue du Loess, BP 28, F-67037 Strasbourg, France.
§Present address: G.S.I., Planckstr. 1, D-64291 Darmstadt, Germany.

shapes with $\gamma=0°$; and the neutron configurations, being in the upper part of the $h_{11/2}$ shell, tend to favor collective oblate nuclear shapes with $\gamma=-60°$. Both of the associated prolate and oblate potential-energy minima are predicted to have similar energies [7–9]. Recoil isomer tagging was recently employed to correlate prompt and delayed data across a 6-μs, $K^{\pi}=8^{-}$ isomer in ^{138}Gd [10] and establish the prompt rotational band built upon the isomer. The selective power of recoil isomer tagging, like that of proton tagging, can be demonstrated by the fact that even when the energies of the prompt ''above-isomer'' transitions are known it remains almost impossible to isolate these transitions in the prompt γ-γ coincidence data due to the overwhelming number of competing channels with large cross sections. However, now that the first few γ rays have been established by recoil isomer tagging, high-fold coincidence data from the EUROBALL [11] or GAMMASPHERE [12] large arrays of high-efficiency detectors should provide this selection. This paper reports on the establishment of new states above a known 15-μs isomer in ^{142}Tb [13] and the feeding and decay of a new isomeric state in ^{144}Ho. This measurement represents first observation of excited states in ^{144}Ho. The difficulty in studying these nuclei can be put into perspective by considering that ^{144}Ho and ^{142}Tb are 21 and 17 neutrons away from their respective stable isotopes, ^{165}Ho and ^{159}Tb. It is anticipated that isomer tagging can be selectively applied to many other isomeric nuclei in this region. In this way, it will be possible to bridge the gap in knowledge between those nuclei that can be studied, at the proton dripline using proton-decay tagging, and the less neutron-deficient nuclei that have sufficiently large cross sections such that they can be studied in heavy-ion fusion-evaporation reactions without the requirement of additional channel selection.

II. EXPERIMENT

Moderate-spin states in the very neutron-deficient nuclei, ^{142}Tb and ^{144}Ho, were populated with the ^{54}Fe+^{92}Mo reaction. Two stacked ^{92}Mo foils, of thickness 500 +300 μg/cm^2, were bombarded with ^{54}Fe beams at energies of 236 and 226 MeV from the K130 cyclotron at the University of Jyväskylä, Finland. Prompt γ-ray transitions were detected with the 27 escape-suppressed germanium detectors of the JUROSPHERE II spectrometer that consisted of 15 EUROGAM type I detectors [14] [of efficiency $\approx$70% relative to a standard 76$\times$76 mm NaI(Tl) detector at 1.3 MeV], seven TESSA type detectors [15], and five NORDBALL type detectors [16] (both of relative efficiency $\approx$25%). The absolute photo-peak efficiency of the JUROSPHERE II array was measured to be $\approx$1.5% at 1.3 MeV. The recoiling evaporation residues were separated from the beamlike particles by the RITU gas-filled separator [17]. The flight time of the recoils through RITU was approximately 0.5 μs. At the focal plane of RITU the residues passed through a multiwire proportional counter (MWPC) and implanted into a 16-strip 80$\times$35 mm silicon detector [18]. The Si-strip detector covered approximately 70% of the recoil distribution at the focal plane. Three NORDBALL and two TESSA detectors were placed in a close geometry around the Si-strip detector in order to detect isomeric or delayed γ rays that were emitted within $\approx$50 μs of a recoil arriving at the focal plane. The absolute focal-plane efficiency of these detectors was determined to be $\approx$0.9% at 1.3 MeV.

The data acquisition was triggered for 50 μs by a recoil event in the Si detector. During this 50-μs period, delayed γ rays that were detected at the focal plane, events in the MWPC detector, and previously detected prompt γ rays from JUROSPHERE II were written to tape. The beam current was approximately 2.7 particle-nA at the higher beam energy (236 MeV) and 2.4 particle-nA at the lower beam energy (226 MeV). These beam currents produced a prompt γ-ray rate in JUROSPHERE II of 1.3 kHz, and a Si rate of 3.0 kHz at 236 MeV, and 1.0 kHz and 2.0 kHz, at 226 MeV, respectively. In the experiment, a total of 6×10^6 prompt events were correlated with delayed events in approximately five days of beam time at 236 MeV and 4×10^5 prompt events in approximately one day at 226 MeV. Energy and efficiency measurements were performed with calibrated ^{133}Ba, ^{152}Eu, and ^{60}Co radioactive sources placed both at the JUROSPHERE II target position and at the Si detector position for the focal-plane germanium detectors.

III. DATA ANALYSIS AND RESULTS

The analysis was performed using a series of two-dimensional matrices and the UPAK [19] software package. In particular, at each beam energy, a recoil-gated γ-γ matrix was created, which contained only those prompt events that were detected in JUROSPHERE II in coincidence with a recoiling nucleus in the Si detector. The main channels populated at 236 MeV were measured to be 26% ^{144}Dy (from the $2p$ evaporation channel), 54% ^{143}Tb ($3p$), 11% ^{142}Gd ($4p$), 8% ^{140}Gd ($\alpha 2p$), and 3% ^{141}Tb (αp). Similarly at 226 MeV, the main channels populated were 47% ^{144}Dy ($2p$), 44% ^{143}Tb ($3p$), 3% ^{142}Gd ($4p$), 4% ^{140}Gd ($\alpha 2p$), and 3% ^{141}Tb (αp).

These data were also sorted into a series of prompt (γ ray detected in JUROSPHERE II) versus delayed (γ ray detected at focal plane) coincidence matrices with various constraints on the time of the delayed γ ray, after a recoiling nucleus was implanted into the Si detector. These matrices allowed correlation of prompt and delayed data across isomeric states. In order to extract lifetimes for the isomeric states, a matrix was constructed of delayed γ-ray energy against the time that the delayed γ ray as measured by the delayed-γ versus recoil time to amplitude converter (TAC). This TAC was started by a recoil event in the Si detector and stopped by a delayed γ ray detected in the focal-plane germanium detectors. In the analysis, many new delayed transitions were observed with half-lives in the nano to microsecond (ns$-\mu$s) range. The most strongly selected transitions in this work were assigned to the decay of the known 15-μs isomer in ^{142}Tb [13] and a new isomeric state in ^{144}Ho.

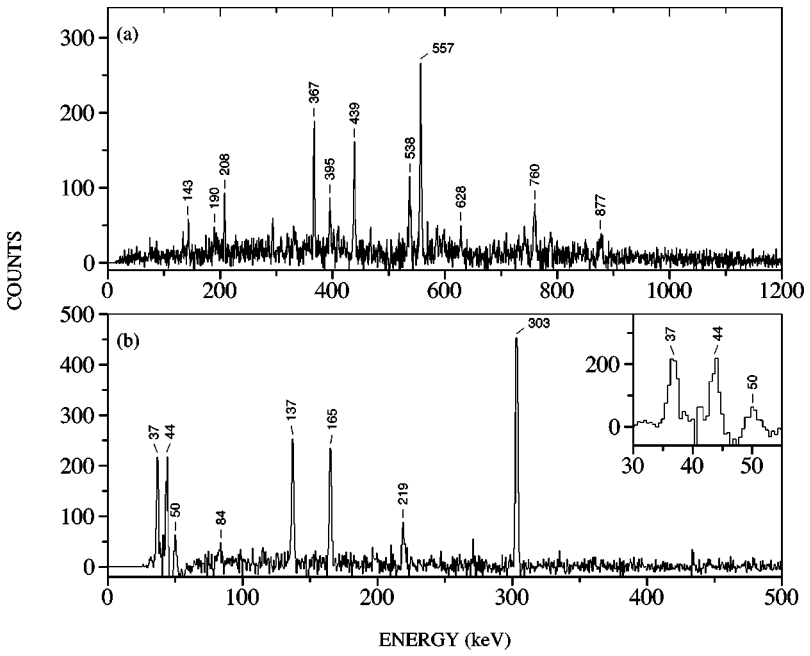

FIG. 1. (a) A spectrum of prompt γ-ray transitions that results from setting gates on 137-, 165-, and 303-keV delayed γ rays from the decay of the 15-μs isomeric state in ^{142}Tb. (b) Spectrum of delayed γ-ray transitions from setting gates on 367-, 439-, 538-, and 557-keV prompt γ rays that feed the 15-μs isomeric state in ^{142}Tb from the 236-MeV data. The inset shows the x-ray region expanded for clarity.

A. ^{142}Tb

The main γ rays that dominate the delayed spectra, in the lifetime range from 10–30 μs at the higher beam energy 236 MeV, were the 37-, 137-, 165-, 219-, and 303-keV transitions, which are known decays from the 15-μs isomer in ^{142}Tb [13,9]. ^{142}Tb was produced through the $3pn$ exit channel and was strongly observed at the higher beam energy that was optimized to the three-particle exit channels. A similarly gated spectrum from the lower beam energy data (226 MeV) showed little evidence for these transitions.

By correlating prompt and delayed γ rays across the isomeric state [10], the structure that feeds the isomer was observed. Gates set on the 137-, 165-, and 303-keV transitions on the delayed axis of the prompt-delayed matrix produced a spectrum of new prompt γ rays that lie above the isomer, shown in Fig. 1(a). Conversely, Fig. 1(b) shows the result of gating on some of these new transitions (367-, 439-, 538-, and 557-keV) on the prompt axis of the matrix and projecting out the γ rays that are in delayed coincidence. The inset to Fig. 1(b) shows the low-energy region of the spectrum that has been expanded for clarity. It should be noted that the good low-energy efficiency and resolution of the smaller-volume TESSA and NORDBALL focal-plane detectors allow the K_α and K_β x rays to be detected. (The Tb x-ray energies are $K_{\alpha 1,2}=43.7$ and 44.5 keV, and $K_{\beta 1,2}=50.3$ and 51.7 keV.) These x-ray transitions are reduced in intensity in the prompt spectra that were taken at the target position due to the presence of absorbers on the large-volume EUROGAM detectors. The detection of x rays is a useful property when the delayed radiation is from an unknown nuclide. Table I lists the measured γ-ray energies and intensities for the known delayed transitions in ^{142}Tb [13] and the newly assigned prompt transitions above the 15-μs isomer.

Note that once the prompt transitions have been established above the isomer, it might be expected that the level scheme can easily be constructed by solely using the prompt γ-γ matrix to examine the coincidences. In fact this is not the case as setting these gates in the prompt matrix results in a highly contaminated spectrum. Unfortunately, the 27 detectors of the JUROSPHERE II spectrometer did not yield sufficient statistics to examine threefold coincidences for these weakly populated channels. This point illustrates the selectivity of the recoil isomer tagging technique for isolating isomeric states in channels with low production cross sec-

TABLE I. γ-ray energies for the known delayed transitions in ^{142}Tb [13] and γ-ray energies and intensities for the new prompt transitions above the isomer established in this work. Note that the prompt and delayed transitions are normalized separately in the two sections.

Delayed E_γ(keV)	I_γ
37.0(5)	81(25)
137.4(4)	33(4)
165.3(2)	34(4)
219.3(1)	1(1)
303.4(1)	100(7)
Prompt E_γ(keV)	**I_γ**
143.4(1)	11(2)
189.6(2)	9(3)
207.9(1)	17(4)
367.1(1)	48(2)
395.3(2)	25(1)
439.0(2)	41(1)
537.9(2)	41(3)
557.2(2)	100(7)
628.6(2)	22(6)
759.9(6)	51(2)
876.9(3)	26(4)

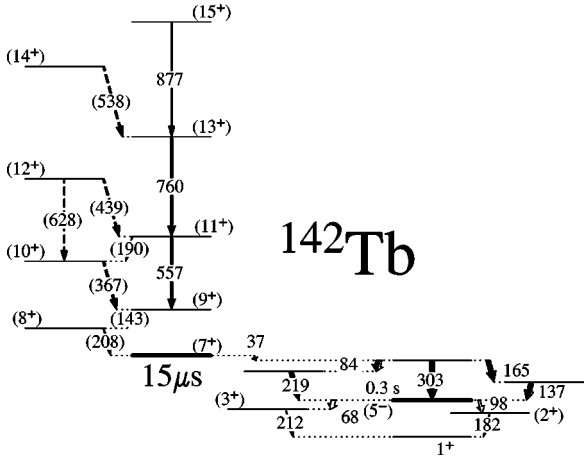

FIG. 2. The deduced level scheme for the states that feed the isomeric state in ^{142}Tb. The white part of the transition arrows indicates the electron-conversion component. The decay of the 0.3 s (5^-) state is from Ref. [9]. The decay of the 15 μs is from Ref. [13].

tions. In order to proceed further, it was necessary to consider the intensities given in Table I and also to construct another gated coincidence matrix of those prompt recoil-gated γ-ray events that were gated by delayed 37-, 137-, 165-, 219-, and 303-keV ^{142}Tb transitions in the lifetime range of 10–20 μs. Although the statistics in this matrix were small, it was still possible to verify that the 557-, 760-, and 877-keV transitions are in coincidence with each other and therefore, likely form a rotational sequence. The other prompt γ rays in Fig. 1(a), 367-, 439-, and 538-keV are tentatively placed as decays into this sequence, see the level scheme for ^{142}Tb, Fig. 2. The tentative placing of these transitions is based upon their intensities, the fact that the energy sums for the 189.6- and 439.0-keV transitions are consistent with the energy of the 628.6-keV transition, and the 439-keV transition was determined to be in coincidence with the 557-keV transition in a recoil-gated prompt γ-γ matrix. This level scheme for ^{142}Tb is consistent with the discussion presented in Sec. IV. The decay of the 15-μs isomer, which was first reported in Ref. [13], was confirmed in this work from the γ-γ coincidences recorded by the focal-plane detectors. The decay of the 0.3-s (5^-) isomeric state was presented in Ref. [9].

B. ^{144}Ho

Figure 3 shows a delayed spectrum measured at the focal plane of RITU produced from the data at both beam energies with the only condition that any γ ray must have occurred 1–3 μs after a recoil was implanted in the Si detector. The main transitions in the spectrum are the 56-, 60-, 148-, and 209-keV γ rays and the 47- and 54-keV x rays. These γ rays were more strongly populated in the 226-MeV data than the 236-MeV data, which implies that they likely arise from a two-particle rather than a three-particle exit channel. The delayed γ-γ matrix from the focal-plane detectors was used to determine the coincidence relations and relative intensities for these transitions but the specific γ-ray ordering remains ambiguous with the present data. The multipolarities of the transitions that depopulate the isomeric state have been deduced from the intensity balance and the internal conversion coefficients. A consistent solution for the decay of the isomer is only found if the 56-, 60-, and 148-keV transitions are of electric dipole character and the 209-keV transition is of electric quadrupole character. This solution is also consistent with the hindered 56-keV γ ray from the isomer being a configuration-changing $E1$ transition.

The use of the recoil isomer tagging establishes which transitions feed these isomeric states. The result of setting gates on the 56-, 60-, 148-, and 209-keV transitions on the delayed axis of the prompt-delayed matrix and projecting out the prompt transitions is shown in Fig. 4(a). The effect of gating on the four most intensely populated prompt γ-ray transitions in this spectrum, 502-, 724-, 856-, and 885-keV and projecting out the delayed γ rays is shown in Fig. 4(b). This spectrum shows the delayed 56-, 60-, 148-, and 209-keV transitions along with the Ho $K_{\alpha 1,2}$ and $K_{\beta 1,2}$ x rays. The inset of Fig. 4(b) shows the x-ray region expanded for clarity. It can be observed that the only x rays in the spectrum correspond very well with those of the unresolved $K_{\alpha 1,2}=47.5$- and 46.7-keV and the resolved $K_{\beta 1,2}=53.8$- and 55.3-keV x rays of Z=67 holmium. The weaker $K_{\beta 2}$

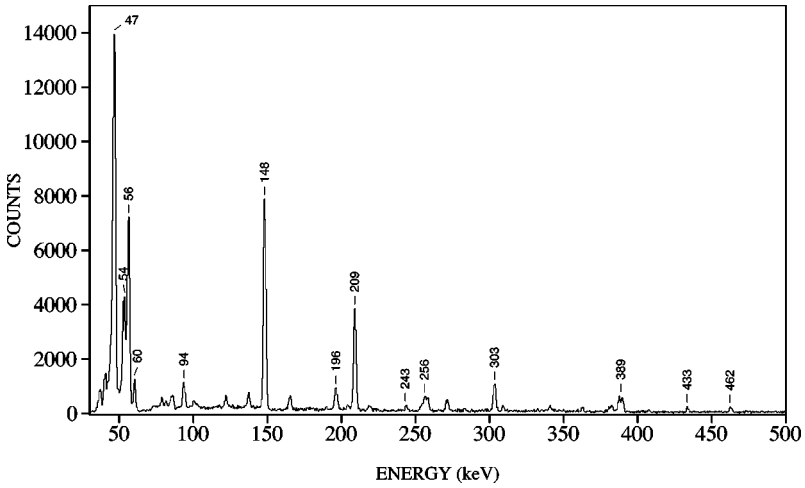

FIG. 3. A γ-ray spectrum gated on the time region of 1–3 μs after a recoil was implanted into the Si detector from the sum of the 226- and 236-MeV data. A long-lived background region has been subtracted.

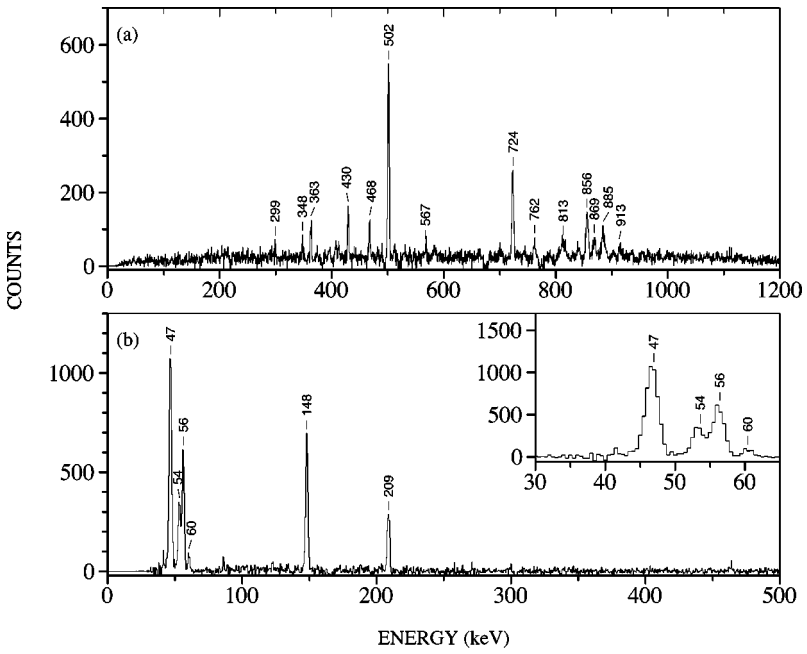

FIG. 4. (a) A spectrum of prompt γ-ray transitions that results from setting gates on the 56-, 60-, 148-, and 209-keV delayed γ rays. (b) Spectrum of delayed γ-ray transitions from setting gates on the 501-, 723-, 856-, and 885-keV prompt γ rays that feed the isomeric state in ^{144}Ho. The inset shows the x-ray region that was used for Z identification. The data are recoil-gated and are from the sum of the 226- and 236-MeV data.

component is hidden by the 56-keV γ ray. This Z information and the fact that these isomeric-decay transitions were more strongly populated in the 226-MeV data than the 236-MeV data, indicate a two- rather than three-particle exit channel, and result in an assignment to the odd-odd nucleus ^{144}Ho from the pn exit channel.

The half-life of the new isomer in ^{144}Ho was established from a series of time spectra gated on the 56-, 60-, 148-, and 209-keV transitions. Figure 5 shows a time spectrum gated by the sum of these transitions from the 226- and 236-MeV data. The least-squares fit to the data yields a half-life of 500(20) ns.

Table II lists the prompt and delayed γ-ray energies and intensities for the newly established transitions in ^{144}Ho. The coincidence relations and ordering of the prompt transitions above the isomer, shown in Fig. 4(a), cannot be determined from the prompt γ-γ matrix from the JUROSPHERE II target array alone. These were deduced from a matrix that only included those prompt recoil-gated γ-ray events that were in coincidence with the delayed 56-, 60-, 148-, and 209-keV

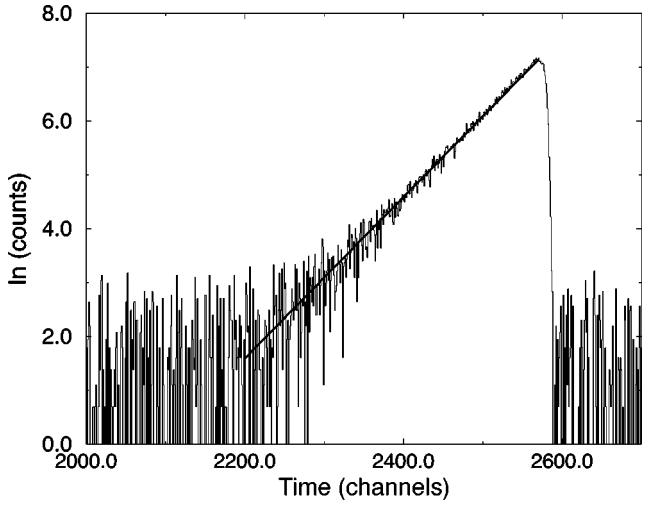

FIG. 5. The lifetime plot for the 500(20)-ns isomeric state in ^{144}Ho and the least-squares fit to the data. The spectrum is the result of a sum spectrum gated on the 56-, 60-, 148-, and 209-keV transitions in the sum of the 226- and 236-MeV data. A local background from the adjacent region to the peak was subtracted from each gate used in the sum.

TABLE II. γ-ray energies and intensities for the transitions assigned to ^{144}Ho in this work. Note that the prompt and delayed transitions are normalized separately in the two sections.

Delayed E_γ(keV)	I_γ
46.7(2) x rays	
53.6(2) x rays	
56.4(2)	100(9)
60.4(3)	11(1)
148.2(2)	91(7)
209.0(2)	54(6)
Prompt E_γ(keV)	**I_γ**
299.1(3)	4(1)
347.5(2)	7(2)
362.9(1)	16(3)
429.6(3)	25(2)
467.8(2)	19(2)
501.6(2)	100(7)
567.3(3)	10(5)
723.6(4)	64(5)
761.7(8)	16(3)
813.1(6)	36(4)
856.0(2)	47(6)
868.5(3)	27(5)
885.2(5)	42(4)
913.0(8)	10(2)

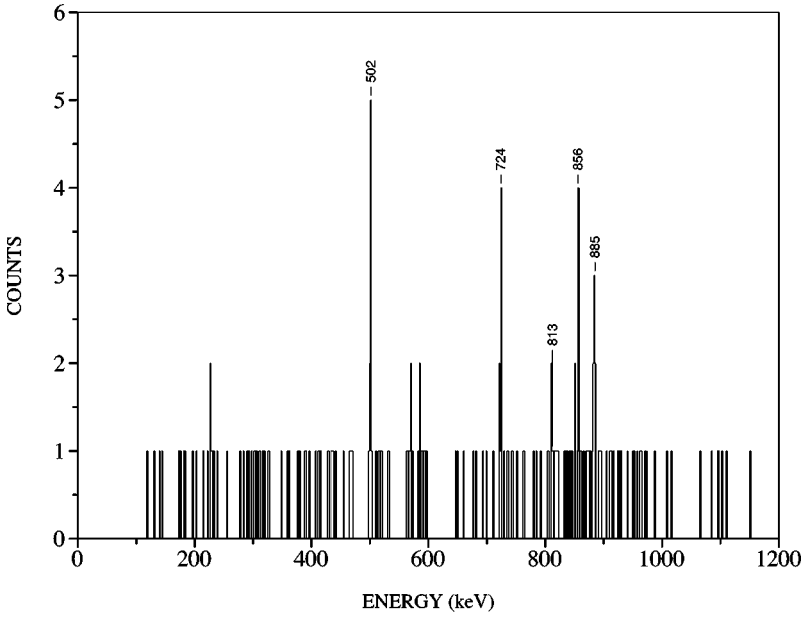

FIG. 6. A sum of the 502-, 724-, and 856-keV prompt gates in a prompt γ-γ matrix that is gated by delayed 56-, 60-, 148-, and 209-keV transitions in the 0.5–2.0-μs time range.

transitions in ^{144}Ho in the lifetime range of 1–3 μs. Although the statistics in this matrix were small, it was still possible to confirm that the 502-, 724-, 856-, 885-, and 813-keV transitions are in coincidence with each other and are likely to form a rotational sequence. Figure 6 shows the sum of the 502-, 724-, and 856-keV gated spectra from this matrix. It was not possible to definitely establish whether the 913-keV transition was also in coincidence with this 502-, 724-, 856-, 885-, and 813-keV transition sequence in these data, but this is likely. In addition, several other prompt γ rays (363-, 430-, and 468-keV) were observed to be in prompt coincidence with the delayed γ rays in ^{144}Ho. The most likely position for these transitions is tentatively shown in the proposed ^{144}Ho level scheme, Fig. 7 and is consistent with the discussion presented in Sec. IV.

Based on the total number of prompt counts in the prompt-delayed spectra for ^{144}Ho [Fig. 4(a)] and ^{142}Tb [Fig. 1(a)], the production cross sections for these bands were estimated to be $\approx$16 μb and $\approx$8 μb, respectively. These values assume total fusion cross sections, predicted from ''evapOR'' [20] based on the code of Ref. [21], of 235 mb and 382 mb at beam energies of 226- and 236-MeV, respectively.

IV. DISCUSSION

The mass 130–140 region of nuclei is well known for exhibiting nuclear shapes that become rather γ soft or triaxial as the neutron number approaches the less deformed region around the $N=82$ shell closure. This loss of axial symmetry makes it difficult to assign specific configurations to particular states as the single-particle nuclear orbits become severely mixed. The underlying reasons for this behavior trend are related to the fact that the protons are in the lower part of the $h_{11/2}$ shell, where prolate deformed shapes are preferred, and the neutrons are in the upper part of the $h_{11/2}$ shell where oblate shapes are preferred. For example, predictions for the holmium nuclei, based on the macroscopic-microscopic mass model of Möller *et al.* [22] and the recent calculations of Rykaczewski *et al.* [3] suggest that ^{143}Ho and ^{141}Ho have a large quadrupole deformation, $\beta_2 \approx 0.29$, ^{145}Ho is only weakly deformed, and ^{147}Ho has a spherical equilibrium shape [3], with a sharp change in nuclear shape from prolate to oblate at ^{144}Ho. Similarly, for the terbium isotopes, the lighter isotopes $^{140-141}$Tb are predicted to have a prolate deformation with a sharp change to oblate deformation at ^{142}Tb. According to Möller *et al.* [22]

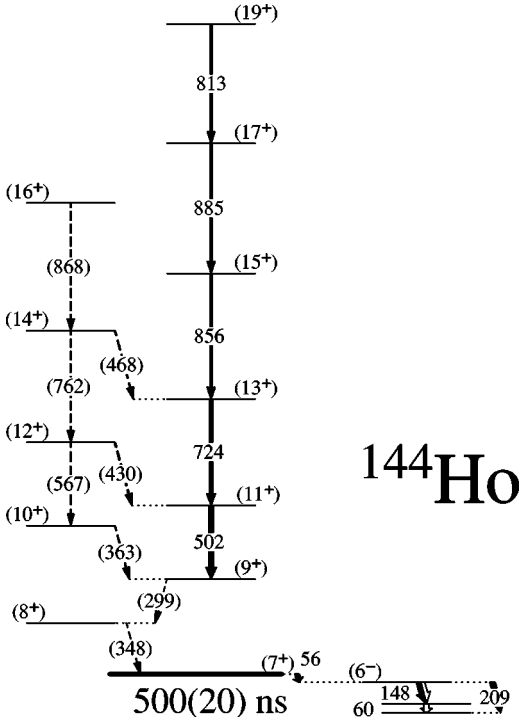

FIG. 7. The level scheme deduced from these data for the states that feed and depopulate the new 500(20)-ns isomeric state in ^{144}Ho. The white part of the transition arrows indicates the electron-conversion component.

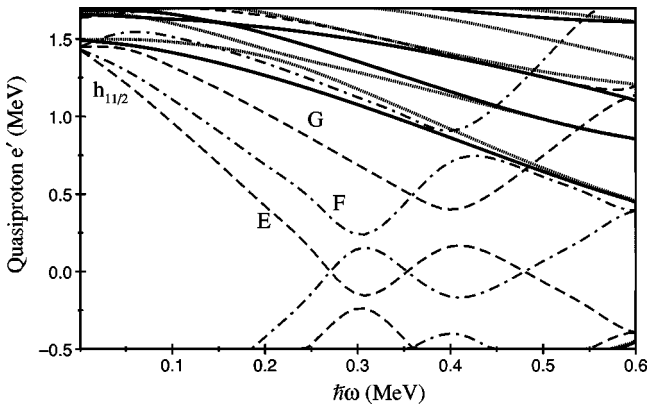

FIG. 8. Representative cranked-shell-model calculation for protons performed for ^{142}Tb with deformation parameters, $\beta_2 = 0.192$, $\beta_4 = -0.022$, and $\gamma = -30°$. The parity and signature (π,α) convention for the lines in the plots are as follows: solid lines refer to $(\pi,\alpha)=(+,1/2)$, dotted lines refer to $(\pi,\alpha)=(+,-1/2)$, dash-dotted lines refer to $(\pi,\alpha)=(-,1/2)$, and dashed lines refer to $(\pi,\alpha)=(-,-1/2)$ quantum numbers.

the two nuclei studied in this work, ^{142}Tb and ^{144}Ho, are the lightest isotopes in each case to show oblate nature and form the $N=77$ boundary between prolate shapes for the lighter isotopes and oblate shapes for the heavier isotopes. However, it should be noted that these calculations do not allow for nonaxial shapes.

In the present work, theoretical total Routhian surface (TRS) and Woods-Saxon cranked-shell-model (CSM) calculations [23] have been performed. The CSM calculations were performed at a deformation extracted from the TRS calculations ($\beta_2 = 0.192$, $\beta_4 = -0.022$, and $\gamma = -30°$) and represent a triaxial nuclear shape. Figures 8 and 9 show the results of this calculation for the protons and neutrons, respectively. This large triaxiality is a consequence of the competition between the different shape-driving effects of the protons and neutrons and is a well-established feature for some of the nuclei in this region, for example, ^{143}Tb($\gamma = -27°$) [24] and ^{139}Pr($\gamma = -15°$) [25]. The large γ deformation is responsible for the large signature splitting of the single-particle orbits and can be observed in Figs. 8 and 9 for the $h_{11/2}$ protons and the $h_{11/2}$ and $f_{7/2}$ neutrons, respectively. A consequence of this large signature splitting is that rotational bands built upon these orbits are expected to form decoupled ($\Delta I = 2$) bands with one signature of the configuration being more favored than the other. Under these triaxial conditions, the individual Nilsson quantum numbers are not conserved, for example, the neutron $h_{11/2}$ orbit will contain substantial components from the $f_{7/2}$ orbit, etc. As a consequence, in the following discussion the configurations will be labeled by the standard convention for parity (π) and signature (α), where E and F refer to $(\pi,\alpha)=(-,-1/2)_1$ and $(-,+1/2)_1$, respectively. The labels G and H refer to $(\pi,\alpha)=(-,-1/2)_2$ and $(-,+1/2)_2$, respectively, and the positive parity labels A and B refer to the $(\pi,\alpha)=(+,+1/2)_1$ and $(+,-1/2)_1$ orbits, respectively.

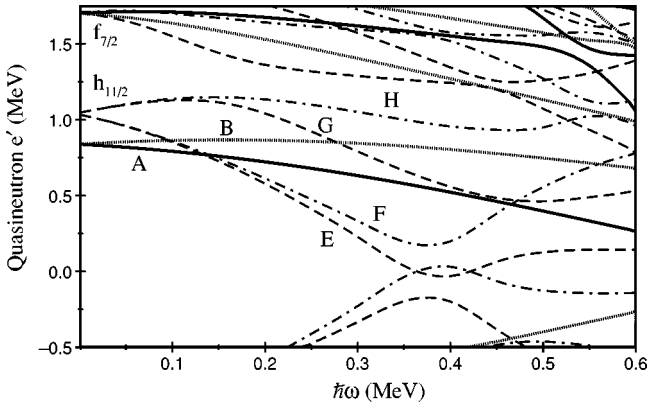

FIG. 9. Representative cranked-shell-model calculation for neutrons performed for ^{142}Tb with deformation parameters, $\beta_2 = 0.192$, $\beta_4 = -0.022$, and $\gamma = -30°$. The parity and signature (π,α) convention for the lines in the plots are as follows: solid lines refer to $(\pi,\alpha)=(+,1/2)$, dotted lines refer to $(\pi,\alpha)=(+,-1/2)$, dash-dotted lines refer to $(\pi,\alpha)=(-,1/2)$, and dashed lines refer to $(\pi,\alpha)=(-,-1/2)$ quantum numbers.

The low statistics for these recoil isomer tagged data do not permit unambiguous spins and configurations to be assigned for the bands established in this work. For example, it would have been useful to consider angular correlation ratios to assign transition multipolarities and therefore, spins to the states. Such information may be obtainable from the large multidetector arrays now that the first few transitions have been established in this work. However, in order to understand the underlying configurations of the isomeric states in ^{144}Ho and ^{142}Tb, it is instructive to consider the properties of the states above the isomers which from these data appear to form collective rotational bands whose nature is dominated by the presence of the proton-$h_{11/2}$ orbits. To test these ideas, the rotational bands built upon the isomeric states in ^{144}Ho and ^{142}Tb have been systematically compared with other $h_{11/2}$ rotational bands in the neighboring nuclei. (The systematics of the $N=78$ odd-proton nuclei ^{137}Pm, ^{139}Pm, and ^{141}Eu were recently discussed in Ref. [24].)

Figure 10 shows the aligned angular momentum (or alignment), i_x [26] versus rotational frequency for the above-isomer rotational bands in ^{144}Ho (consisting of the 502-, 724-, 856-, 885-, and 813-keV transitions) and ^{142}Tb (consisting of the 557-, 760-, and 876-keV transitions) from this work with that of the neighboring odd-mass $h_{11/2}$ bands in ^{145}Ho [27], ^{143}Tb [24], ^{139}Eu [28], and ^{141}Eu [29]. The bands in ^{144}Ho and ^{142}Tb have both been plotted with an isomer band-head spin of $7\hbar$ and a $K=5\hbar$. These values are assumed to be the most likely spins based on the available orbits around the Fermi surface shown in Figs. 8 and 9 and also the likely multipolarities for the delayed transitions based on intensity arguments. [Notice the similarity of the decay schemes for ^{144}Ho and ^{142}Tb above the (5^-) state in ^{142}Tb.] In Fig. 10, the ^{143}Tb band [24] is observed to gain alignment at 0.38 MeV and again at 0.44 MeV. The alignment gain $\Delta i_x = 4\hbar$ at 0.38 MeV was interpreted as the first allowed proton-band crossing (the so-called FG proton crossing) involving the second and third protons since the configuration of this band is based on the first proton $\pi h_{11/2}$ E orbital being occupied [24]. Other bands whose configura-

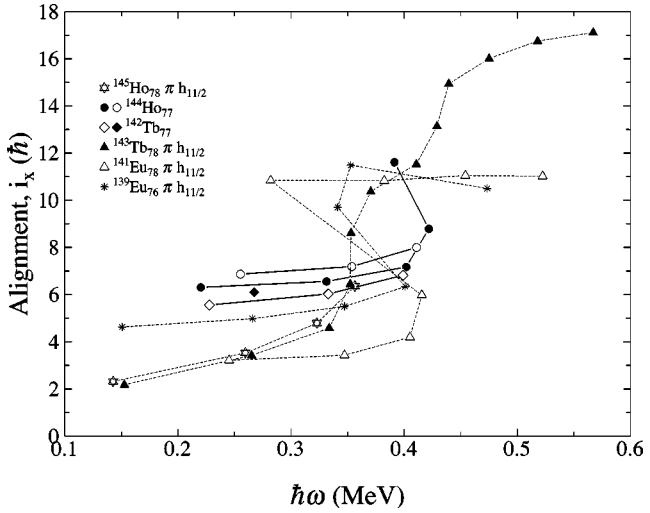

FIG. 10. The aligned angular momentum, i_x versus rotational frequency for the rotational bands in ^{144}Ho and ^{142}Tb from this work (see text for details) compared with that of the neighboring odd-mass $h_{11/2}$ bands in ^{145}Ho [27], ^{143}Tb [24], ^{139}Eu [28], and ^{141}Eu [29]. A reference band with Harris parameters [30] $\Im_0 = 12.0\hbar^2\text{MeV}^{-1}$ and $\Im_1 = 25.0\hbar^4\text{MeV}^{-3}$ [29] was subtracted from all data in the figure.

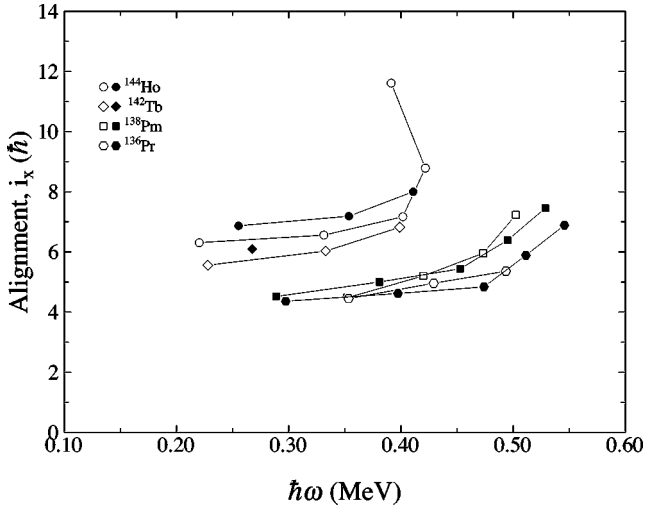

FIG. 11. The aligned angular momentum i_x versus rotational frequency for the $\pi h_{11/2} \otimes \nu h_{11/2}$ bands in the $N=77$ isotones. A reference band with Harris parameters [30] $\Im_0 = 12.0\hbar^2$ MeV^{-1} and $\Im_1 = 25.0\hbar^4$ MeV^{-3} [29] was subtracted from all data in the figure.

tions are based on this $\pi h_{11/2}$ proton E orbit are shown for ^{145}Ho, ^{139}Eu, and ^{141}Eu. These bands show similar alignment gains at 0.37 MeV although the europium isotopes exhibit a weaker mixing strength. Figure 10 shows that the behavior of the band built upon the isomeric state in ^{144}Ho is similar (albeit with a slightly higher crossing frequency that is likely related to the different deformation). The higher crossing, at 0.44 MeV, was interpreted as the first allowed neutron crossing $\nu(EF)$ in ^{143}Tb [24]. Unfortunately, in the present data set for ^{144}Ho there were not sufficient statistics to verify the γ-ray coincidences and ordering of the transitions above the 813-keV γ ray and therefore, the total alignment gain could not be established. In a similar manner, the values for ^{142}Tb appear to lie along the same locus as the points for the other bands based on the first $h_{11/2}$ proton orbit. The coincidence relationships for the ^{142}Tb band do not allow this band to be extended into the band-crossing region. However, they appear to show the start of a slight upturn between 0.3 and 0.4 MeV. Due to these similarities, these new bands above the isomers in ^{142}Tb and ^{144}Ho are reasoned to have the same underlying $\pi h_{11/2}$ proton E configuration as their neighboring nuclei coupled to the lowest neutron configuration νE or νA, i.e., $\pi h_{11/2} \otimes \nu(h_{11/2}, f_{7/2})$ or $\pi h_{11/2} \otimes \nu(s_{1/2}, d_{3/2})$ configurations.

Strongly coupled bands, based on the $\pi h_{11/2} \otimes \nu h_{11/2}$ configuration, were recently observed in ^{140}Tb [31]. The differences between these bands in ^{140}Tb and the bands in ^{142}Tb and ^{144}Ho are consistent with those expected for the larger triaxiality and smaller deformation in the heavier nuclei [22]. This triaxial interpretation is also consistent with the systematic trend observed for other $N=77$ $\pi h_{11/2} \otimes \nu h_{11/2}$ bands where a sharp change in behavior is predicted [22] for the heavier isotones ^{142}Tb and ^{144}Ho. Figure 11 shows the alignment for the known $\pi h_{11/2} \otimes \nu h_{11/2}$ bands in the $N=77$ isotones. In the figure, the bands in ^{142}Tb and ^{144}Ho show a larger signature splitting than those in ^{136}Pr [32] and ^{138}Pm [33]. Notice that the alignment for the strongly coupled bands in ^{136}Pr and ^{138}Pm have adjacent points midway between each other compared with the decoupled, presumably more triaxial, bands in the heavier nuclei ^{142}Tb and ^{144}Ho that show a shift from the midpoint. A decoupled $h_{11/2}$ ground-state band was also recently observed in ^{141}Ho [34] with a large signature splitting.

V. CONCLUSIONS

Two new bands built upon the isomeric states in ^{144}Ho and ^{142}Tb show a behavior that is consistent with that expected from deformed nuclei with a large triaxiality. Their underlying single-particle configurations are likely composed of $\pi h_{11/2} \otimes \nu(h_{11/2}, f_{7/2})$ or $\pi h_{11/2} \otimes \nu(s_{1/2}, d_{3/2})$ states. In order to fully determine the underlying configuration, the observation of the full-band crossings, which was not possible with the current experimental setup, would be required. Now that the low-spin transitions have been identified by a recoil isomer tagging technique, an experiment with one of the current state-of-the-art large multidetector arrays, such as EUROBALL [11] or GAMMASPHERE [12] should provide sufficient resolution and high-fold statistics to extend these bands built upon the isomers and to find additional bands. It is expected that recoil isomer tagging will play a major role in identifying nuclei in this region and thereby bridge the gap in knowledge between the proton emitters and the less neutron-deficient nuclei that can be studied by heavy-ion fusion-evaporation reactions with stable beam and target combinations without the requirement of additional channel selection.

ACKNOWLEDGMENTS

The authors would like to thank H.-Q. Jin for the use of the ''JINWARE'' plotting routines. JUROSPHERE II is jointly funded by the EPSRC and IN2P3. Support for this work was provided by the Academy of Finland and the Large Scale Facility program under the TMR program of the European Union. Six of us (A.J.B., H.C.S., C.F., S.L.S., M.C., and J.G.N.) acknowledge EPSRC. D.M.C. also acknowledges the support of the EPSRC. The EUROGAM detectors were provided from the UK/France EPSRC/IN2P3 loan pool. The NORDBALL detectors were provided by the Niels Bohr Institute, Denmark.

[1] P.J. Woods and C.N. Davids, Annu. Rev. Nucl. Part. Sci. **47**, 541 (1997).
[2] C.N. Davids *et al.*, Phys. Rev. Lett. **80**, 1849 (1998).
[3] K. Rykaczewski *et al.*, Phys. Rev. C **60**, 011301(R) (1999).
[4] E. Maglione, L.S. Ferreira, and R.J. Liotta, Phys. Rev. Lett. **81**, 538 (1998).
[5] E. Maglione, L.S. Ferreira, and R.J. Liotta, Phys. Rev. C **59**, R589 (1999).
[6] C.N. Davids *et al.*, Phys. Rev. C **55**, 2255 (1997).
[7] R. Broda *et al.*, Z. Phys. A **321**, 287 (1985).
[8] N. Redon *et al.*, Z. Phys. A **325**, 127 (1986).
[9] R. B. Firestone *et al.*, preprint LBL-26591, 1989.
[10] D.M. Cullen *et al.*, Phys. Rev. C **58**, 846 (1998).
[11] P.J. Nolan, F.A. Beck, and D.B. Fossan, Annu. Rev. Nucl. Part. Sci. **45**, 561 (1994).
[12] I.Y. Lee, Nucl. Phys. **A520**, 641c (1990).
[13] I. Zychor *et al.*, GSI Report No. 89-1, 1989.
[14] C.W. Beausang *et al.*, Nucl. Instrum. Methods Phys. Res. A **313**, 37 (1992).
[15] P.J. Nolan, D.W. Gifford, and P.J. Twin, Nucl. Instrum. Methods Phys. Res. A **236**, 95 (1985).
[16] B. Herskind, Nucl. Phys. **A447**, 395 (1985).
[17] M. Leino *et al.*, Nucl. Instrum. Methods Phys. Res. B **99**, 653 (1995); M. Leino, *ibid.* **126**, 320 (1997).
[18] P.J. Sellin *et al.*, Nucl. Instrum. Methods Phys. Res. A **311**, 217 (1992).
[19] W. T. Milner, *The Holifield Heavy Ion Research Facility Computer Handbook* (Oak Ridge National Laboratory, Tennessee, 1987); (private communication).
[20] J. R. Beene, *''EvapOR''; the Oak Ridge Data Analysis Package* (Oak Ridge National Laboratory, Tennessee, 1999); (private communication).
[21] A. Gavron, Phys. Rev. C **21**, 230 (1980).
[22] P. Möller, J.R. Nix, W.D. Myers, and W.J. Swiatecki, At. Data Nucl. Data Tables **59**, 185 (1995).
[23] W. Nazarewicz, R. Wyss, and A. Johnson, Nucl. Phys. **A503**, 285 (1989).
[24] F.R. Espinoza-Quiñones *et al.*, Phys. Rev. C **60**, 054304 (1999).
[25] N. Xu, C.W. Beausang, E.S. Paul, W.F. Piel, Jr., and D.B. Fossan, Phys. Rev. C **36**, 1649 (1987).
[26] R. Bengtsson and S. Frauendorf, Nucl. Phys. **A314**, 27 (1979); **A327**, 139 (1979).
[27] R. B. Firestone, *Table of Isotopes*, 8th ed, edited by V. S. Shirley (Wiley, New York, 1996).
[28] P. Vaska *et al.*, Phys. Rev. C **52**, 1270 (1995).
[29] N. Xu, C.W. Beausang, J.R. Hughes, Y. Liang, R. Ma, E.S. Paul, W.F. Piel, Jr., S. Shi, and D.B. Fossan, Phys. Rev. C **43**, 2189 (1991).
[30] S.M. Harris, Phys. Rev. **138**, B509 (1965).
[31] M.A. Rizzutto *et al.*, Phys. Rev. C **62**, 027302 (2000).
[32] C.M. Petrache *et al.*, Nucl. Phys. **A603**, 50 (1996).
[33] U. Datta Pramanik *et al.*, Nucl. Phys. **A632**, 307 (1998).
[34] D. S. Seweryniak *et al.*, Phys. Rev. Lett. (submitted).